Fourier Transform Infrared and Quasielectron Neutron Scattering Studies on the Binding Modes of Methanol Molecules in the Confined Spaces of HMCM-41 and HZSM-5: Role of Pore Structure and Surface Acid Sites

Narendra M. Gupta,*,†,‖ Dharmesh Kumar,†,⊥ Valmik S. Kamble,† S. Mitra,‡ R. Mukhopadhyay,‡ and V. B. Kartha§

Applied Chemistry and Solid State Physics Divisions, Bhabha Atomic Research Centre, Trombay, Mumbai - 400 085, and 21, Udaigiri, Sion-Trombay Road, Mumbai - 400088

Received: July 5, 2005; In Final Form: October 24, 2005

Quasielastic neutron scattering (QENS) and Fourier transform infrared spectroscopic studies were carried out on methanol molecules adsorbed in HMCM-41 and HZSM-5 molecular sieves to monitor the effect of pore structure on their occluded state under the conditions of ambient temperature and 5−250 mbar pressures. The QENS results have shown that the pore geometry of the host matrix and the dipolar character of the adsorbate are together responsible for the binding state of guest molecules in the confining medium. Thus, neither translational nor free rotational motion was noticed for methanol molecules adsorbed in HZSM-5, in contrast to benzene and cyclohexane molecules of almost similar size that are reported to undergo a rotational motion under the identical conditions of loading (*Phys. Chem. Chem. Phys.* **2001**, *3*, 4449; **2003**, *5*, 3066). In the case of HMCM-41, a translational motion of occluded methanol molecules was clearly observed with a diffusion constant $D \approx 1.5 \times 10^{-5}$ cm^2 s^{-1}, as compared to a value of $D \approx 2.6 \times 10^{-5}$ cm^2 s^{-1} for its liquid state. These results indicate that the adsorbed methanol experiences a considerable extent of supercooling due to capillary condensation in zeolitic pores, giving rise to formation of a metastable state even at room temperature. In HZSM-5, entrapped methanol exists in an almost solidlike state, whereas in HMCM-41, its density lies between that of the solid and the liquid phases. Infrared spectroscopic study conducted using deuterium-labeled adsorbate and host matrixes have given evidence for different kinds of interactions between the methanol molecules and the host matrix, depending upon the loading. For small loadings the internal hydroxy groups within the pore system get perturbed first, giving rise to formation of the methoxy groups. Multilayer adsorption and capillary condensation of methanol occur for a loading of 0.05 mmol per gram and above, within the pore system and also at the external surface, giving rise to a highly compressed state due to strong intermolecular bonding. At the same time, a considerable amount of exchange occurred between the hydroxy groups of the adsorbed methanol and those of the host matrix. Such exchange of hydroxy groups may play an important role in the catalytic properties of the porous aluminosilicates.

I. Introduction

The thermodynamic and transport properties of some fluids are known to alter considerably on their physical confinement in the well-defined channels and cavity systems of porous aluminosilicate materials.[1] Many issues such as the role played by the zeolitic pore structure and the influence of the chemical nature of adsorbate in the overall molecular motions in such porous media, however, continue to be a frontline area of research. In previous investigations reported from our laboratory, we have employed in situ Fourier transform infrared spectroscopy (FTIR) and quasielastic neutron scattering (QENS) techniques to demonstrate that small molecules, such as carbon monoxide, benzene, and cyclohexane, exist in a highly compressed nonequilibrium state when occluded at room temperature in the channels/cages of micro- and mesoporous aluminosilicates.[2−12] For instance, it has been established that on adsorption in HZSM-5 zeolites at room temperature benzene molecules transform into a state, the density of which lies between that of the liquid and the solid phases, depending upon the loading. In this state, benzene molecules are found to be packed with their planes parallel to zeolitic walls and experience a strong intermolecular interaction through π electron clouds. Furthermore, the intermolecular bonding in this occluded phase of benzene depends considerably on the pore geometry of the host matrix.[4−7]

In continuation of these studies, we have now investigated the adsorption of methanol in the channels of ZSM-5 and MCM-41 molecular sieves using methodologies mentioned above. Our objective was to gain some fundamental understanding of the pore size effect on the dynamics of polar molecules occluded in aluminosilicate matrixes, under the reaction conditions close to that in actual practice. In addition, the interaction of methanol with aluminosilicates is of considerable technological importance. It is well known that methanol as a C_1 source can be converted to certain value-added products, such as high-octane gasoline or light olefins, utilizing the catalytic role of the zeolitic

* To whom correspondence should be addressed. E-mail: nm.gupta@ncl.res.in.

† Applied Chemistry Division, Bhabha Atomic Research Centre.

‡ Solid State Physics Division, Bhabha Atomic Research Centre.

§ Udaigiri.

‖ Current address: Catalysis Division, National Chemical Laboratory, Homi Bhabha Road, Pune - 411008, India.

⊥ Current address: University of Vermont, Department of Chemistry, Burlington, VT 05405.

10.1021/jp053668e CCC: $33.50
Published on Web 02/18/2006

TABLE 1: Physical Characteristics of the Adsorbent Samples

sample	Si/Al	surface area ($m^2\ g^{-1} \pm 5\%$)	pore diameter[a] (Å)	pore volume (mL/g ± 10%)
HMCM-41	~30	1020	28	0.91
SiMCM-41		951	28	0.90
HZSM-5	~30	410	5.6	0.28

[a] As per DHK formula.

acid sites. With this in view, we have complemented our study by using CH_3OD molecules as adsorbate and also some deuterated molecular sieve samples as an adsorbent so as to monitor the host−guest and the adsorbate−adsorbate interactions involved in this adsorption process.

II. Experimental Section

Materials. Ammoniated form of ZSM-5 zeolite (Si/Al ratio ≈ 30) was obtained from the Associated Cement Companies Ltd, Thane, India. Samples of HZSM-5 zeolite were prepared by calcining the sample at 773 K for 6 h. HMCM-41 sample, with Si/Al ratio of 30, was synthesized by the method described in the literature,[13] using fumed silica (99%, Fluka), cetyl trimethylammonium bromide (Merck), trimethylammonium hydroxide (25% in water, Fluka), and aluminum isopropoxide (97%, Fluka). A similar procedure was adopted for synthesizing a siliceous MCM-41 sample as well. The structural and the compositional properties of the synthesized samples, monitored by powder X-ray diffraction and differential thermal analysis/thermal gravimetric analysis techniques, were found to match well with those reported in the literature. The surface area, pore volume, and pore size were determined by N_2 adsorption method using Sorptomatic model-1990 analyzer from C. E. Instruments, Italy. Table 1 gives the salient physical characteristics of the different samples.

Extra-pure AR-grade methanol (SISCO Research Laboratories, Mumbai, India) was distilled before use to remove any moisture contamination. CH_3OD (99.5 at. % D, Aldrich) was used without any further treatment.

A JASCO (Japan) model-610 FTIR spectrophotometer equipped with a DTGS detector was employed for recording of the IR absorption spectra in transmission mode. A self-supporting sample wafer of 25 mm diameter and weighing ~16 mg cm^{-2} was mounted in an IR cell (~100 mL volume) fitted with water-cooled CaF_2 windows.[8,9] The sample wafer was subjected to a pretreatment at 623 K under vacuum (10^{-4} Torr) for 24 h and then cooled to the desired temperature. A background spectrum was recorded at this stage. The sample was then exposed to different amounts of methanol vapor ranging from 0.025 to 1.25 mmol g^{-1} of adsorbent, and the spectra were recorded at different intervals of time. A mixture containing ~0.25 mol % of methanol in argon was employed for introducing methanol vapor in the cell. The gas pressure in the IR cell after the introduction of methanol vapor + argon was in the range of 5−250 mbar for the doses mentioned above. Scans (300) were co-added for collecting each spectrum, with a resolution of 4 cm^{-1}. The data were finally plotted taking spectrum of the corresponding bare sample wafer as background to observe clearly the spectral features arising due to methanol loading. All the IR data reported in the text represent such difference spectra, unless mentioned otherwise. Accordingly, the IR bands pointing downward in the figures, i.e., with the negative value of absorbance, indicate the perturbation or removal of a particular molecular group of the adsorbent.

The deuteroxylated molecular sieve wafers were obtained by in situ heating of the sample at 575 K in the presence of deuterium gas, followed by cooling and evacuation. This process was repeated several times until OD groups replaced the majority of the functional OH groups. Such samples prepared from MCM-41 and ZSM-5 wafers are referred to as MCM-OD or ZSM-OD, respectively, in the text.

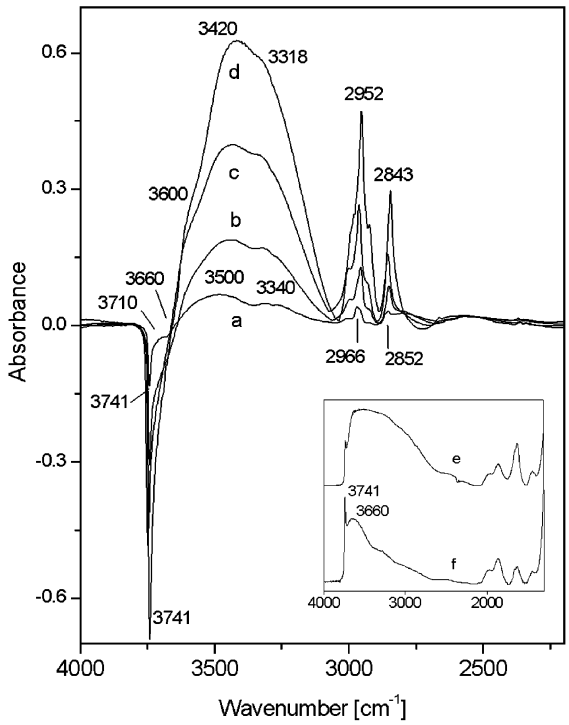

Figure 1. Difference IR spectra of HMCM-41 (Si/Al = 30) wafer, exposed in situ to increasing doses of CH_3OH. (a) 0.05, (b) 0.25, (c) 0.50, and (d) 1.25 mmol g^{-1}. Inset figure shows IR spectra of pure unexposed HSM-5 sample with no background subtraction, without (curve e) and after in situ activation at 550 K (curve f).

QENS Studies. The details of the spectrometer and the procedure adopted in the study are described elsewhere in detail.[14] The neutron-scattering experiments were performed using a neutron-scattering spectrometer installed at Dhruva reactor, Trombay. The spectrometer is used in multiangle reflecting crystal (MARX) mode, where one essentially uses a combination of large analyzer crystal and a linear position sensitive detector, providing larger throughput. This spectrometer has an energy resolution of 200 μeV with an incident energy of 5.1 meV. The quasielastic spectra were recorded in the wavevector transfer (Q) range of 0.8−1.8 $Å^{-1}$ at 300 K. With the energy resolution available in this spectrometer, diffusion constants of the order of 10^{-5}−10^{-6} $cm^2\ s^{-1}$ could be measured.

About 1.7 g of HZSM-5 or 0.7 g of HMCM-41 sample was placed in a thin wall (2 mm) aluminum cell of rectangular shape (100 mm × 12 mm). The sample thickness was around 4 mm. A transmission of more than 92% assured negligible multiple scattering effects. The samples were heated for 48 h at 625 K under vacuum (~10^{-6} mbar) prior to their exposure to methanol. Methanol loadings in HZSM-5 and MCM-41 samples were ~6 and ~20 mmol g^{-1}, respectively, so as to achieve a saturation filling of the pores.

III. Results

Methanol Adsorption in HMCM-41. Figure 1 shows the difference spectra of the MCM-41 wafer, recorded at beam temperature as a function of methanol loading after subtracting the blank pellet spectrum. In the inset of this figure are shown the IR spectra of an unexposed wafer for comparison, recorded

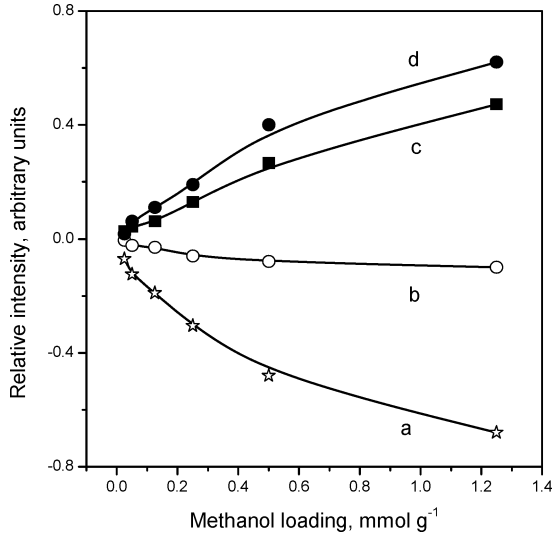

Figure 2. The effect of loading on the relative intensity of some prominent vibrational bands developed on adsorption of CH_3OH in MCM-41. (a) 3741, (b) 3660, (c) 2952, and (d) 3420 cm^{-1}.

with air as reference, prior to (curve e) and after degassing for 20 h at 600 K (curve f). A comparison of these results helps us in highlighting the following features:

(i) The broad and overlapping IR bands at 3741 and 3668 cm^{-1} in Figure 1f are the characteristic ν(OH) bands of dehydrated HMCM-41, the frequency of which is known to depend on the Si/Al ratio and calcination temperature.[15−17] These two bands represent the well-reported isolated terminal silanols and the hydroxy groups located inside the channels and identified as Si−OH−Al groups associated with the octahedrally coordinated aluminum oxide species. The broad band appearing at ∼3500 cm^{-1} in an uncalcined sample (Figure 1e) arises from the hydrogen bonded water molecules occluded in the channels of MCM matrix and are easy to remove on thermal activation.[15] The intensity of both the bands at 3741 and 3668 cm^{-1} (Figure 1f) decreased progressively with an increase in the amount of methanol introduced, the effect being more pronounced on the 3741-cm^{-1} band, particularly for the higher doses of methanol. The change in the relative intensity of these bands is depicted in curves a and b of Figure 2. The frequencies of different bands remained almost unchanged irrespective of the methanol loading.

(ii) Additional overlapping bands were observed in the ν(OH) region, peaking at around 3600, 3550, and 3340 cm^{-1}. These bands shifted progressively to marginally lower frequencies with increase in methanol loading (parts a−d of Figure 1) and differ from the ν(OH) bands of physisorbed water molecules (Figure 1e). Also, the frequency and the nature of these overlapping IR bands differ from the ν(OH) bands of liquid methanol and liquid water in their adsorbed state, as is apparent from the comparative data given in Figure 3. These IR bands in the 3600−3000-cm^{-1} region may be identified with the vibrations of H-bonded methanol with significant intermolecular interaction due to their occlusion in the channels of MCM matrix. It is likely that the presence of different clustered states of methanol may contribute to these overlapping bands.

(iii) Typical methoxy (−OCH_3) group bands are observed in the aliphatic C−H stretching region, with frequency maxima at 2952 and 2843 cm^{-1} along with the shoulder bands appearing at around 2980 and 2923 cm^{-1}. While the intensity of these bands increased, their frequency was found to decrease progressively with the increase in the amount of methanol dosed. Curves c and d in Figure 2 show the comparative growth behavior of 2952- and 3420-cm^{-1} vibrational bands.

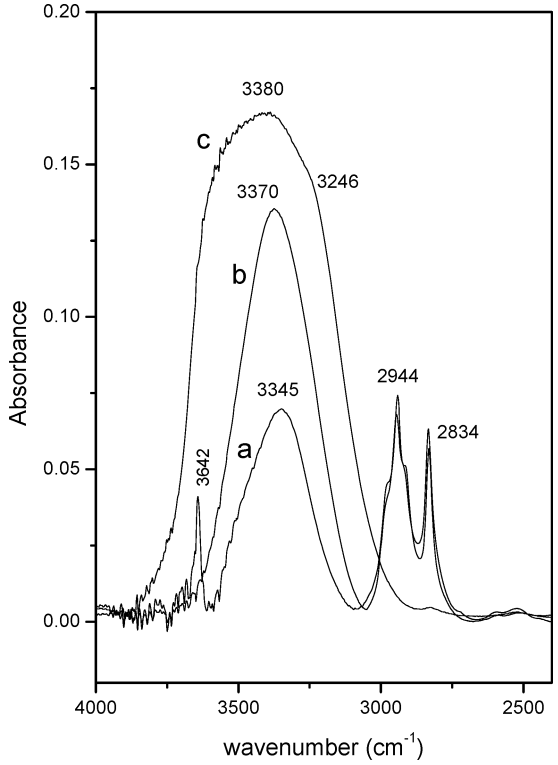

Figure 3. Stretching region vibrational bands for (a) CH_3OH, (b) CH_3OH (10%) + CCl_4, and (c) H_2O, when adsorbed in a KBr wafer.

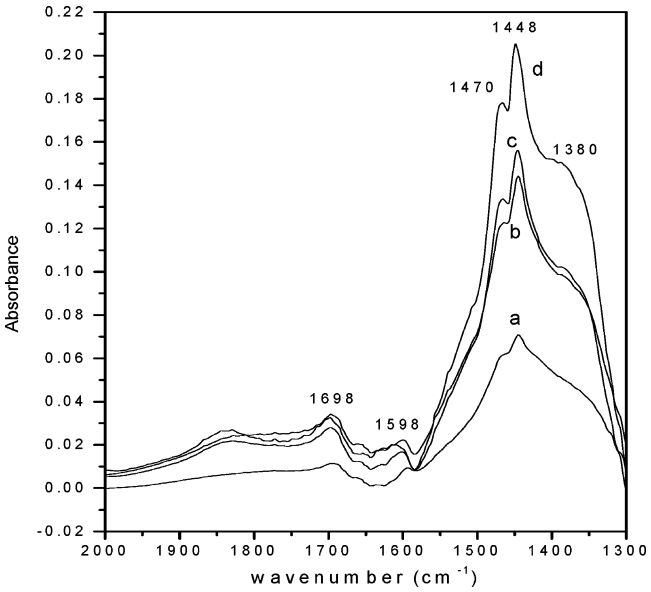

Figure 4. Bending region vibrational bands of CH_3OH adsorbed in MCM-41 at different loadings: (a) 0.05, (b) 0.25, (c) 0.50, and (d) 1.25 mmol g^{-1}.

(iv) In the C−H deformation region, we observed overlapping broad bands at 1468, 1450, and 1398 cm^{-1} that are characteristic of the liquid phase of methanol (Figure 4). A near absence of δ(OH) vibration at ∼1650 cm^{-1} in this figure confirms a negligible contribution of adsorbed water in the 3600−3000-cm^{-1} region bands mentioned above (Figure 1)

Figure 5 presents the IR spectra for adsorption of CH_3OD in MCM-41. We observe here the changes in ν(OH) bands similar to those in Figure 1 and also a growth of C−H stretching bands in the 3100−2800-cm^{-1} region as a result of methanol loading. At the same time overlapping broad bands are observed in the ν(OD) region, with maxima at around 2656, 2528, and 2444

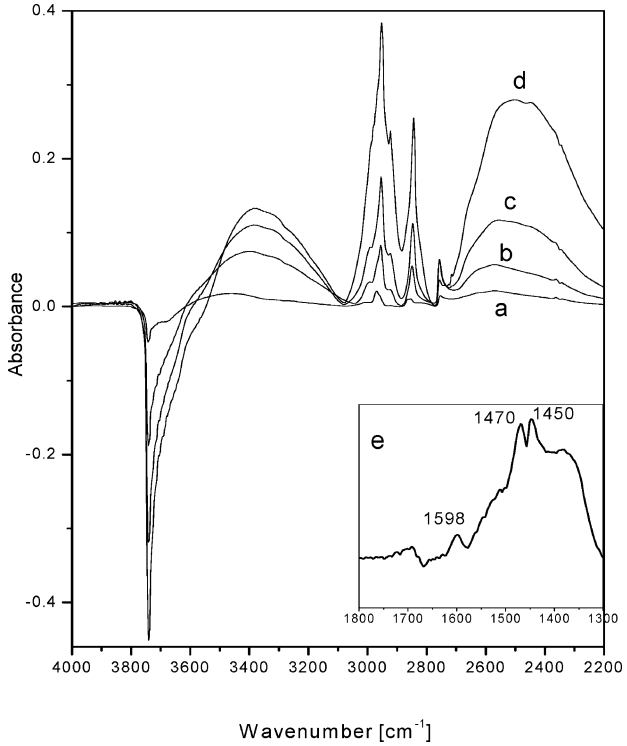

Figure 5. Difference IR spectra of HMCM-41, exposed in situ to increasing doses of CH_3OD: (a) 0.05, (b) 0.25, (c) 0.50, and (d) 1.25 mmol g^{-1}. Curve e in the inset shows the bending region spectrum corresponding to curve c.

cm^{-1} (parts a−d of Figure 5), corresponding to 3600-, 3420-, and 3318-cm^{-1} bands in Figure 1 and as per the expected isotopic shift $\nu(OD)/\nu(OH) \approx 0.737$. It is also of interest to note the presence of ν(OH) bands at maxima of 3382 and 3240 cm^{-1}, their intensity increasing with the loading of CH_3OD (parts b−d of Figure 5). We also take note of a sharp ν(OD) band at 2758 cm^{-1} in Figure 5, the intensity increasing again with the loading. These results reveal clearly an exchange/scrambling of OH and OD bands between the host and the adsorbate molecules.

This inference is validated from the spectral features depicted in Figure 6 for the adsorption of CH_3OH over MCM-OD sample, i.e., a sample having OH groups substituted with OD. We see very clearly the progressive growth of the 3740-cm^{-1} band with the increase in CH_3OH loading. At the same time, significantly intense bands are observed in the 2500−2300-cm^{-1} region due to condensed CH_3OD, particularly for higher loadings of methanol (parts c and d of Figure 6). These results confirm again the exchange of the hydroxy/deuterioxy groups, as mentioned above.

In accordance with the above-mentioned observations, dosing of CH_3OD over MCM-OD resulted in a sharp negative ν(OD) band at 2758 cm^{-1}, along with the growth of the vibrational bands arising due to condensed state of CH_3OD (cf. Figure 5). These results are presented in Figure 7.

We may mention that the C−H region bands at 2952 and 2843 cm^{-1} due to the methoxy groups remained by and large unaffected, irrespective of the methanol loading and the isotopic substitutions described above.

Adsorption over SiMCM-41. A trend, similar to that described above, was observed in the IR spectra recorded for siliceous MCM-41 samples after adsorption of CH_3OH or CH_3OD vapor at room temperature. Thus, we observed a progressive removal of ν(OH) bands corresponding to SiMCM-41

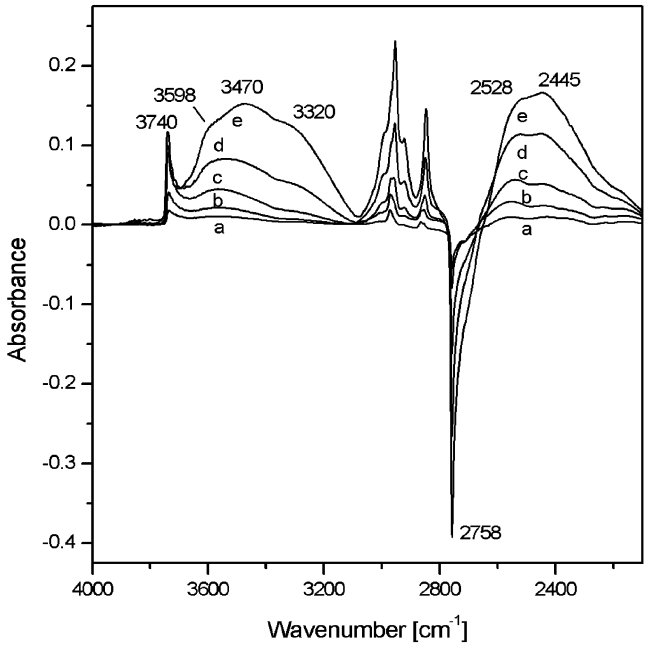

Figure 6. Difference IR spectra of HMCM-OD sample, exposed in situ to increasing doses of CH_3OH: (a) 0.05, (b) 0.25, (c) 0.50, and (d) 1.25 mmol g^{-1}.

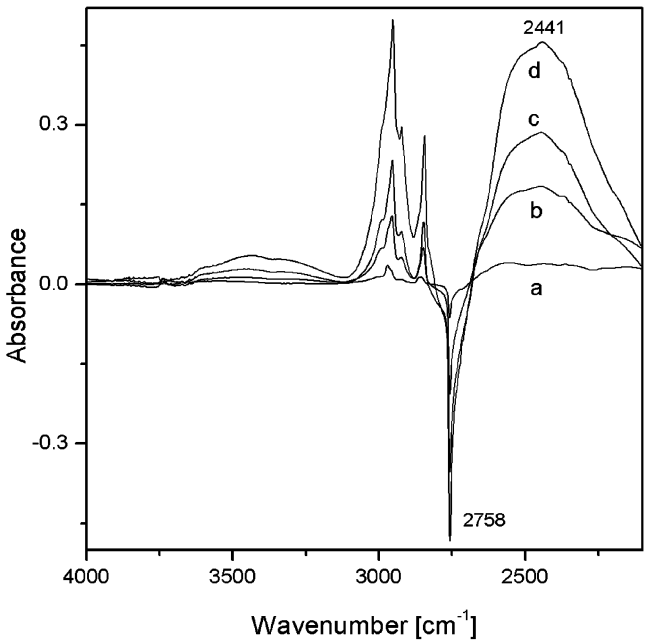

Figure 7. Difference IR spectra of HMCM-OD sample exposed in situ to increasing doses of CH_3OD: (a) 0.05, (b) 0.25, (c) 0.50, and (d) 1.25 mmol g^{-1}.

as a result of increasing methanol loading, accompanied with the growth of methoxy group bands and also the bands in 3000−3100 cm^{-1} or alternately 2700−2200-cm^{-1} region bands due to occluded CH_3OH or CH_3OD molecules in a condensed state.

Adsorption over HZSM-5. Figures 8 and 9 depict the IR spectra of HZSM5 wafer, exposed to different doses of CH_3OH and CH_3OD, respectively, and recorded at beam temperature. As in the case of MCM, the introduction of increasing amount of methanol resulted in disappearance of all the stretching region bands of silanol or the bridge-bonded OH groups, characteristic of HZSM-5 (see Figure 8e and refs 18 and 19), depending upon the amount of methanol dosed. Thus, while the 3612-cm^{-1} band experienced a perturbation even for the smallest amount of

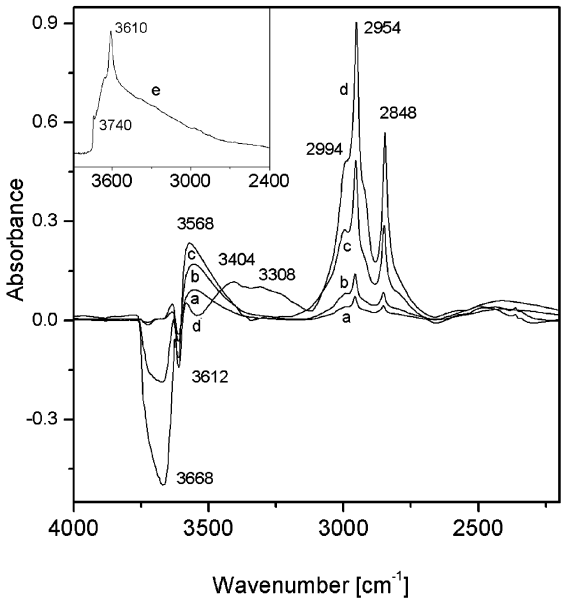

Figure 8. Difference IR spectra of HZSM-5 after contacting with increasing amounts of CH_3OH: (a) 0.05, (b) 0.25, (c) 0.50, and (d) 1.25 mmol g^{-1}. Curve e shows IR spectrum of degassed HZSM-5, recorded with air as reference.

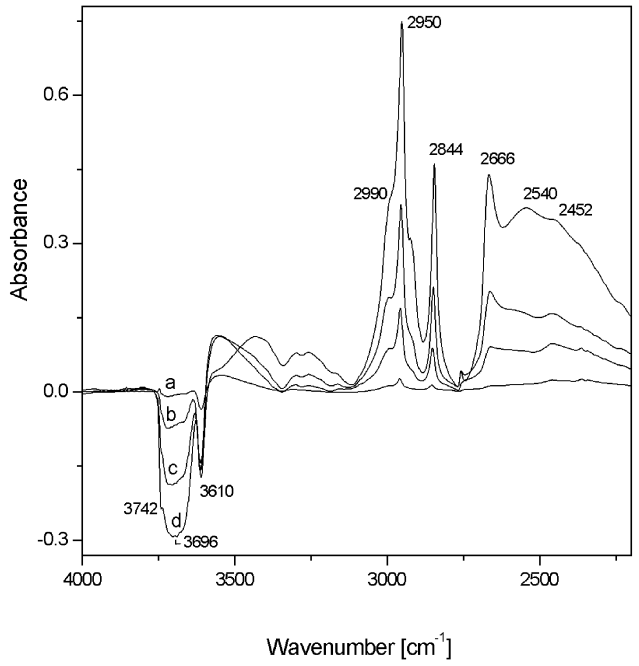

Figure 9. Difference IR spectra of HZSM-5 after contacting with increasing amount of CH_3OD: (a) 0.05, (b) 0.25, (c) 0.50, and (d) 1.25 mmol g^{-1}.

methanol dosed, the intensity of the higher frequency bands at 3740 and 3668 cm^{-1} was affected only at higher loadings. The removal of these ν(OH) bands was accompanied by the appearance of a broad band at around 3568 cm^{-1} for loading of CH_3OH in range of 0.025−1.25 mol g^{-1}, the intensity increasing progressively with the loading (parts a−c of Figures 8). The intensity of this band however registered a decrease with further increase in the methanol loading and a new pair of bands was observed at lower frequencies of 3404 and 3308 cm^{-1} (Figure 8d). The bands in the C−H stretching region (3100−2800 cm^{-1}) due to methoxy groups are also noticed in these figures, their frequency shifting again to lower values as a function of loading.

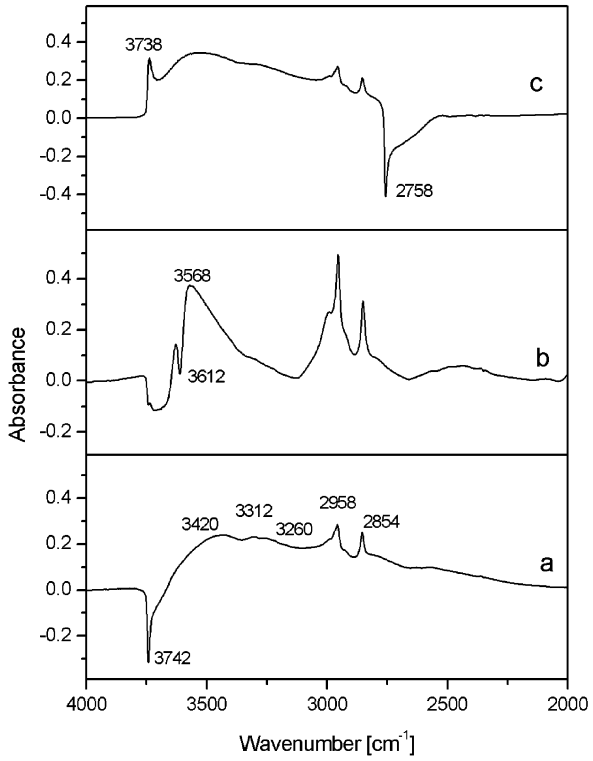

Figure 10. IR spectra of MCM-41 (curves a and c) and ZSM-5 (curve b) samples, exposed to 2.50 mmol g^{-1} of CH_3OH (curves a and b) or CH_3OD (curve c), followed by degassing for about 20 min.

A similar trend was observed in the IR results for adsorption of CH_3OD over HZSM-5 (Figure 9). It is of interest to notice in Figure 9 that, in addition to overlapping ν(OD) bands at 2666, 2540, and 2452 cm^{-1}, we observe weak bands in the corresponding ν(OH) region as well, particularly for the higher loadings of methanol (parts b−d of Figure 9), in support of the experiments carried out using CH_3OH.

Effect of Degassing. Figure 10 presents the IR spectra of MCM-41 (curves a and c) and ZSM-5 (curve b) sample wafers, exposed to CH_3OH (curves a and b) or CH_3OD (curve c) followed by degassing for ∼20 min. These results reveal that the IR bands due to condensed methanol were removed almost completely in the case of the MCM sample (parts a and c of Figure 10), while in the case of ZSM-5, the IR band at 3568 cm^{-1} appears to be more stable under the identical conditions (Figure 10b). We similarly observe the ease of removal of methoxy group C−H bands in case of the methanol-loaded MCM samples, as compared to ZSM-5. We also notice that the intensity of the silanol group bands decreased only by ∼50% on degassing, and no significant changes were observed on further evacuation at room temperature. These results clearly reflect on the important role of pore geometry on the stability of the methanol phases occluded in the zeolitic pores.

QENS Studies. In a neutron-scattering experiment the scattered intensity is analyzed as a function of both energy and momentum transfer $Q = (4\pi \sin \theta/\lambda)$, where 2θ is the scattering angle. The quantity measured is the double differential scattering cross section ($d^2\sigma/\partial E \partial\Omega$), which represents the probability that a neutron is scattered with energy change dE into the solid angle dΩ,[20]

$$\frac{d^2\sigma}{\partial\omega\partial\Omega} \propto \frac{k}{k_0}[\sigma_{coh}S_{coh}(Q,\omega) + \sigma_{inc}S_{inc}(Q,\omega)] \qquad (1)$$

$S(Q,\omega)$ is known as the scattering law and the subscripts coh

and inc denotes the coherent and incoherent components. k and k_0 are the final and initial wavevectors. $Q = k - k_0$ is the wavevector transfer and $\hbar\omega = E - E_0$ is the energy transfer. Incoherent scattering involves the same nucleus at two successive times, so there are no interference effects between the amplitudes scattered by different nuclei. In the case of hydrogenous systems, such as methanol, the total scattering of neutrons is dominated by the incoherent scattering of protons since σ_{coh} (any element) $\ll \sigma_{inc}$ (proton). Therefore, in the case of neutron scattering from methanol we can write

$$\frac{d^2\sigma}{\partial\omega\partial\Omega} \propto \frac{k}{k_0}[\sigma_{inc}S_{inc}(Q,\omega)] \tag{2}$$

In general, the incoherent scattering law can be written as[21]

$$S_{inc}(Q,\omega) \propto A(Q)\delta(\omega) + [1 - A(Q)]L(\Gamma,\omega) \tag{3}$$

where the first term is the elastic part and the second term is the quasielastic part. $L(\Gamma,\omega)$ is a Lorentzian, and Γ is the half width at half-maximum (HWHM) of the Lorentzian function inversely related to the time constant of the motion. It is convenient to analyze the data in terms of elastic incoherent structure factor (EISF), which provides the information about the geometry of the molecular motions. If $I_{el}(Q)$ and $I_{qe}(Q)$ are the elastic and quasielastic intensities, respectively, the EISF is defined as[20]

$$\text{EISF} = \frac{I_{el}(Q)}{I_{el}(Q) + I_{qe}(Q)} \tag{4}$$

Therefore, $A(Q)$ in eq 3 is nothing but the EISF.

Adsorption in MCM-41. The QENS spectra from the dehydrated and unexposed MCM-41 did not show any quasielastic broadening over the resolution function of the instrument. This indicates that the hydroxy groups present in a sample are not labile and do not contribute to the QENS data, at least in the time window of our spectrometer. However, significant broadening was observed from the sample loaded with methanol, and this may therefore be attributed exclusively to the molecular motions of adsorbed species. To explore the contribution of occluded molecule, the QENS spectrum of bare molecular sieves was subtracted from the spectrum of the loaded sample. The data thus obtained were analyzed following an unbiased procedure, where no specific model was assumed. Elastic and quasielastic components in the total spectra at all Q values were estimated. The model scattering law given in eq 3 was convoluted with the instrumental resolution, and the parameters ($A(Q)$ and Γ) were determined by least-squares fit to the data. It was found that the elastic component ($A(Q)$) is almost zero for all the Q values, suggesting that the observed dynamics does not involve any elastic part and one Lorentzian function explains the data quite well. One Lorentzian function convoluted with the resolution function is fitted to the total spectra, and the fit was shown in Figure 11 at some typical Q values. These reasonably good fits indicate that the observed QE broadening corresponds only to the translational motion of the adsorbed molecules. The rotation of the adsorbed molecules could be either very fast or very slow to be observed in the time domain of the present measurements. The data points related to the HWHM values of the Lorentzian functions, as obtained from the fit, are given in Figure 12. To arrive at an understanding of the dynamics of methanol molecules in the pores of MCM-41, we now compare these data with some plausible models. When a molecule, such as methanol, performs translational motion in a confined space, different models can be envisaged to describe its motion. The simplest motion can be thought of is the Brownian motion, where it is assumed that the particles move under the influence of the forces arising from the collisions between them. Between the two collisions, particles move in a straight line. After a collision it goes to another random direction, independent of the previous one. In this case, incoherent scattering law can be calculated by solving the Fick's law[20] and written as

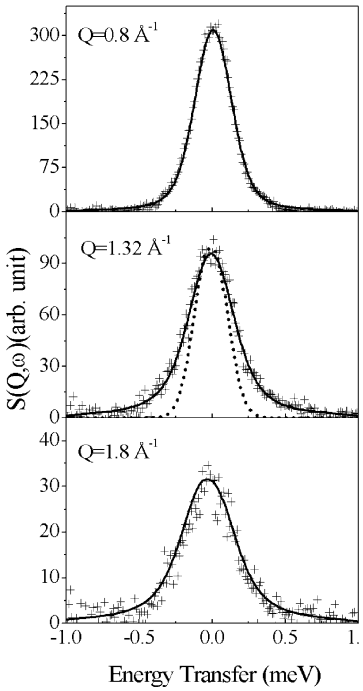

Figure 11. Typical QENS spectra at some Q values for methanol adsorbed in MCM-41. Spectra are fitted with one Lorentzian function convoluted with the resolution function. Solid lines represent the fitted lines, and dotted lines represent the instrument resolution function.

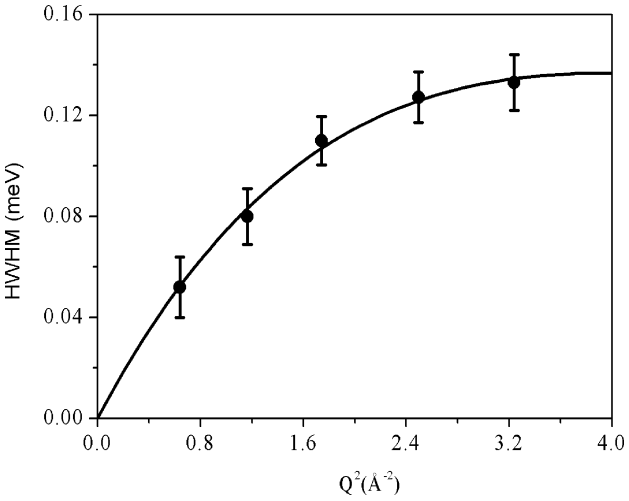

Figure 12. Variation of HWHM with Q^2 for methanol adsorbed in MCM-41. Solid line is the fit with Chudley−Elliott model.

$$S_{inc}(Q,\omega) = \frac{1}{\pi}\frac{DQ^2}{\omega^2 + (DQ^2)^2} \tag{5}$$

The scattering law exhibits a Lorentzian shape whose HWHM increases with the momentum transfer according to a DQ^2 law

TABLE 2: Comparison of the Dynamical Parameters for Translational Motion of Various Molecules Adsorbed in MCM-41 According to the Chudley−Elliott Model

adsorption in MCM-41	molecular diameter (Å)	dipole moment (debye)	jump length ($\langle l \rangle$, Å)	residence time (τ, ps)	diffusion constant = $l^2/6t$ (10^{-5} cm^2/s) when adsorbed in MCM-41	bulk liquid diffusion constant (10^{-5} cm^2/s) at room temperature
methanol	4.5	1.7	2.3 ± 0.6	5.8 ± 0.5	1.5 ± 0.1	2.6
benzene	5.8	0	3.1 ± 0.3	7.5 ± 0.6	2.2 ± 0.6	2.2
cyclohexane	6.0	0	2.4 ± 0.7	5.7 ± 0.7	1.7 ± 0.4	1.7

TABLE 3: Comparison of the Dynamical Parameters for Rotational Motion of Various Molecules Adsorbed in HZSM-5

adsorption in HZSM-5	model	residence time (ps) when adsorbed in HZSM-5	residence time for bulk solid (ps)	residence time for bulk liquid at room temperature (ps)
methanol	no broadening seen			10.2
benzene	6-fold jump rotation	16.5	19.2 at 277 K	2.5
cyclohexane	3-fold jump rotation	8.2	6.0 at 180 K	1.7

and provides a direct method of determining the diffusion constant. However, as can be seen from Figure 12, HWHM of the quasielastic component deviates from the linear behavior at high Q values that suggests that simple Fick's law is not adequate in describing the experimental data and we need to describe the diffusion process in more detail. One such model was formulated by Chudley and Elliott.[22] This model assumes that, for a time interval τ (referred to as residence time), a particular molecule remains on a given site, vibrating about a center of equilibrium. After this time, the molecules move rapidly to another site, in a negligible jump time. The jump length l is assumed to be the same for all such jumps under consideration. This model is also called a fixed jump model. The powder averaged scattering law in this case can be written as

$$S_{\text{inc}}(Q,\omega) = \frac{1}{\pi}\frac{\Gamma(Q)}{\omega^2 + (\Gamma(Q))^2} \tag{6}$$

where

$$\Gamma(Q) = \frac{1}{\tau}\left[1 - \frac{\sin Ql}{Ql}\right] \tag{7}$$

One can also find out the diffusion constant, D, from Einstein's relation

$$D = \frac{l^2}{6\tau} \tag{8}$$

In Figure 12, also shown is the fit of the HWHM values of the Lorentzians as per the Chudley−Elliott model. As seen in Figure 12, the experimental values fit quite well with this model. The values of residence time (τ), jump length ($\langle l \rangle$), and the diffusion constant (D) obtained from the fitting in Figure 12 are indicated in Table 2. Also included in this table are similar data for adsorption of benzene and cyclohexane under identical corrections, so as to enable us to compare the binding behavior of some small molecules of almost similar size but different polarity. On comparing the D value given in Table 2 with the value reported for the diffusion constant of liquid methanol at 298 K ($D = 2.4$ or 2.6×10^{-5} cm^2/s),[23,24] we may conclude that the translational diffusion constant of methanol entrapped in MCM-41 is much less than that of the bulk liquid methanol. On the contrary, in the case of benzene and cyclohexane molecules adsorbed in MCM-41, the value of diffusion constant is almost similar to that obtained for corresponding bulk liquid samples (see Table 2).[25,26] In consideration that the physical dimensions of the three molecules are similar and that the stearic hindrance may not play a very crucial role, the QENS results in Table 2 point to an important contribution of the polar nature of methanol molecules. We can visualize that, not only a greater intermolecular bonding in the case of nonpolar molecules such as benzene and cylohexane, molecular symmetry plays an important role in deciding their diffusion parameters such as jump lengths, residence time as indicated in Table 2.

Adsorption in HZSM-5. Dehydrated HZSM-5 zeolite, as in the case of MCM sample, did not show any broadening over the instrumental resolution. Methanol adsorption in HZSM, however, gave very different results compared to many other small hydrocarbon molecules. Thus, in contrast to significant quasielastic broadening observed for adsorption of benzene and cyclohexane in HZSM-5 zeolite, indicating the mobility of these molecules in the channels, no quasielastic broadening was seen for the methanol vapor adsorbed in this sample. Figure 13 showed the typical QENS spectra at $Q = 1.32$ Å^{-1} along with the instrumental resolution for methanol adsorbed in the HZSM-5 sample. It is clear that no quasielastic broadening was observed in case of methanol adsorbed in HZSM-5 sample, in contrast to what observed in methanol adsorbed in MCM-41 sample. This indicates that no motion in the time scale of 10^{-10}−10^{-12} ps is occurring in the methanol-adsorbed HZSM-5 sample. Different dynamical parameters for adsorption of methanol benzene and cyclohexane in HZSM-5 are given in Table 3 for comparison.

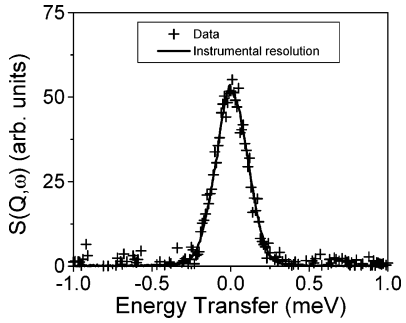

Figure 13. Typical QENS spectra at $Q = 1.32$ Å^{-1} along with the instrumental resolution for methanol adsorbed in HZSM-5 sample. No quasielastic broadening is seen.

IV. Discussion

The QENS and IR results described above present certain interesting features that are different from a number of earlier studies, reported on the adsorption of methanol in aluminosilicates at low coverages.[27−30] The preponderance of electronic interaction of methanol with the framework sites, leading thereby to formation of methoxy groups, both at silicon and aluminum sites has been amply highlighted in these studies. Our data on the other hand reveal that a close intermolecular interaction is

predominant at coverage under this study, leading thereby to occlusion of a clustered or a condensed phase of methanol, the nature of which depended upon not only the pore geometry or the chemical composition of the confining medium but also on the polarity of the guest molecules.

Following are the highlights of our studies:

1. 3750−3650-cm^{-1} Region Bands. We observe that the IR bands in this ν(OH) region, and also corresponding ν(OD) bands, experience considerable decrease in intensity but no shift in their frequency irrespective of the amount of methanol dosed. A similar trend is noticed in the vibrational bands in the 2700−2600-cm^{-1} region (Figures 6 and 7). It is thus likely that, whereas the framework hydroxyl groups, both in HZSM-5 and HMCM-41, may participate in the reaction, no direct electronic interaction may occur between the adsorbed CH_3OH molecules and the Al^{3+} or the charge-balancing cations. This is corroborated by the similarity of our IR results obtained for siliceous and Al-containing MCM-41 samples, as mentioned above.

2. 3600−3300-cm^{-1} Region Bands. The multiple vibrational bands observed in this region are often interpreted in term of the shift of higher frequency ν(OH) bands due to interaction of CH_3OH with the framework hydroxyl groups and the extent of this shift is regarded as a measure of the strength of zeolite−methanol interaction.[27,28] We may however mention that ν(OH) bands in this region also appear because of H−H bonding of methanol molecules leading thereby to a polymeric or a condensed phase. The results of our study are in full support of this assignment. First, the peak width at half height and the relative intensity of the overlapping bands, peaking at ∼3600, 3420, and 3318 cm^{-1} in Figure 1, are quite different from the corresponding ν(OH) bands in the 3750−3650-cm^{-1} region. As seen from Figure 2, the decrease in the intensity of isolated Si−OH corresponds to increase in methanol loading (bands 3420 and 2952 cm^{-1}), while the 3660-cm^{-1} band shows very little change, confirming that the O−H groups associated with octahedrally coordinated species are relatively unaffected. The data in Figures 5 and 6 provide useful clue in this regard. These data show that a progressive decrease in the intensity of ν(OH) vibrations of framework hydroxyl groups is accompanied by the development of ν(OD) bands corresponding to condensed CH_3OD and weak bands in the 3600−3300-cm^{-1} region. These observations also confirm an exchange of the hydroxyl groups between methanol and framework OH groups. A part of $(CH_3OH)_n$ formed in the process gets occluded in the zeolitic cages along with $(CH_3OD)_n$, as is evident from the presence of 3600−3300-cm^{-1} bands in Figures 5, 8, and 9. We may also mention that the H_2O molecules that are likely to be generated during the process of methoxy formation may not contribute significantly to the vibrational bands observed in this region, as is apparent from the absence of δ(OH) band in the spectra shown in Figures 4 and 5e.

Such condensation of methanol molecules in the confined medium of aluminosilicates has been predicted in previous theoretical and experimental studies as well. For instance, based on ab initio SCF MO studies, Pelmenschikov et al.[31] have demonstrated the formation of large hydrogen-bonded polymers of methanol molecules in silicate, even at high concentration of unoccupied −SiOH groups. These authors have compared the calculated and observed frequencies to show that, at low coverage, methanol bonds to silica site, while at high coverage the physically adsorbed methanol tends to form cyclic hydrogen bonded polymers with the participation of the −SiOH group.[31] The broad vibrational bands at 3300 and 3440 cm^{-1} developed on adsorption of methanol on ZSM-5 at pressures exceeding to10^{-3} mbar have been assigned to the formation of large adsorption clusters with only weak intermolecular hydrogen bonding.[19] Similarly, Hunger et al.[32] employed temperature-programmed desorption and adsorption measurements to demonstrate the nonspecific interaction of methanol molecules in ZSM-5 zeolites and formation of strong hydrogen bonds in the methanol clusters at higher loadings. That there are no free CH_3OH molecules in the zeolite systems can be seen from Figure 3, where a 10% methanol solution in CCl_4 shows the 3640-cm^{-1} O−H band, corresponding to hydroxy groups that are not hydrogen bonded.

The QENS results show that this process of condensation in zeolitic materials is influenced considerably by pore geometry of the host matrix and also by the polarity of the entrapped molecules. Thus, almost no translational and rotational motions of methanol molecules in the channels of HZSM-5 indicate the presence of a highly confined state, close to a solid state. In the case of MCM, the occluded methanol molecules show translational motion with a diffusion constant of $\sim 1.5 \times 10^{-5}$ cm^2 s^{-1}, as compared to a value of 2.6×10^{-5} cm^2 s^{-1} for the liquid state. This again shows a highly hindered motion of methanol molecules due to capillary condensation.

3. 3000−2800-cm^{-1} Region Methoxy Group Bands. We observe at least two pairs of C−H stretching vibrational bands, one at frequencies of 2952 and 2843 cm^{-1} and the other at 2980 and 2923 cm^{-1}. These bands experience a frequency shift to a varying extent of almost nil to 21 cm^{-1} as a function of loading. IR bands in this region due to methoxy groups have been reported by several research groups, and again varying assignments have been proposed. In general, it is shown that the methoxy groups may bond at aluminosilicate framework in various coordinations shown below, i.e., at cation site, at silica site alone, or jointly at silica and alumina sites.

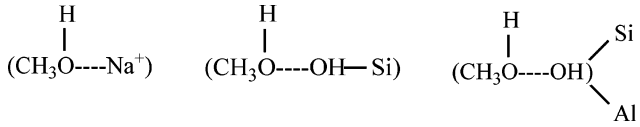

The frequencies of these bands are known to vary marginally with the mode of these bondings. It has also been reported that the C−H stretching bands of these methoxy groups overlap with the vibrational frequencies in this region of hydrogen-bonded polymeric state of CH_3OH molecules.[30,31] Following these earlier reported studies and considering that no major change is observed in the frequency of these bands on isotopic substitutions, either in the host matrix or the guest molecules, we assign them to overlap of methoxy groups due to binding at silica sites as well as the methanol clusters occluded in the zeolitic pores.

On the basis of the points discussed above, we may thus conclude that, while a fraction of methanol molecules are bonded at silica sites, a majority of them give rise to the formation of hydrogen-bonded clusters. IR spectra in Figures 1−6 demonstrate that the clustering of methanol is more pronounced at loadings higher than 5.4 μmol g^{-1} (pressure 10 mbar). The intermolecular binding of methanol in this clustered state depended upon pore structure as well, the binding being stronger for smaller size (5−6 nm) pores of HZSM-5. Spectral features in Figure 10, which show the ease of removal of both the clustered methanol molecules and the methoxy groups from MCM matrix, validate this inference.

Our results are thus in harmony with the previously reported theoretical as well as experimental studies that have demon-

strated the important role of a confining geometry in the modification of the fundamental properties of a fluid and its respective phase transition.[33−37] It is well reported that the liquids confined in very small pores exhibit supercooling well below the free liquid−solid transition temperature. For instance, Ritter et al.[33] employed a picosecond time-resolved optical technique to demonstrate that this supercooled state was remarkably different from that of a free liquid and the dynamics of the occluded fluid mimics that of a solid phase. Zerda and Shao[34] demonstrated that when a liquid is placed in small pores, the freezing temperature is inversely proportional to the pore radius. These authors have estimated that in the case of adsorption of cyclohexane in porous silica the temperature of the liquid solid-phase transition in the 29-Å pore to be equal to 218 K, in the 54-Å pore to be 240 K, and in the 220-Å pore to take place at 280 K. Our results, on the contrary, show that the polar CH_3OH molecules entrapped in the 5−6-Å-sized pores of ZSM-5 may exist in a supercooled and highly compressed state even at room temperature, showing practically no translational and rotational motion (Figure 8). In the larger pores of MCM-41, the values of the residence time and diffusion constant (Tables 2 and 3) indicate the formation of a nonequilibrium physical state, the transport properties of which lie between that of a liquid and a solid state of methanol. Our results appear to corroborate earlier findings that the microscopic clusters of a confined fluid may form at significantly above bulk freezing temperature.[38]

By comparison of these observations with the parallel QENS results for nonpolar molecules such as benzene and cyclohexane (Tables 2 and 3 and refs 3 and 4), we find that in contrast to almost no rotational motion of occluded methanol in HSM-5 the benzene and cyclohexane molecules exhibited a 6-fold and 3-fold rotational motion, respectively, under the identical conditions of temperature, pressure, and loading. It is thus quite evident that the dipolar nature of the sorbate molecules also plays an important role in deciding the physical state of guest moieties in a confining medium.

Our IR results thus demonstrate that the hindrance of the molecular motions due to guest−host interaction may be important only for the monolayer, while in the next layers the freedom of molecular motion may be determined exclusively by the intermolecular interaction between the sorbate molecules and the pressure effect of the zeolitic walls, causing the capillary condensation and the supercooling effect, as mentioned above. The results presented in Figure 10 on postexposure pumping of the sample are in harmony with these inferences and suggest that the removal of a liquid from pores by capillary evaporation is also dependent on the pore dimensions and the nature of the sorbate molecules.[36]

V. Conclusion

In conclusion, the results of present study provide definite evidence that in addition to pore geometry and size of the confining medium the chemical nature and the shape of the guest molecule may also play a crucial role in controlling the physical state of an occluded phase, a fact that has been overlooked in many of the previous studies on this subject.[33]

References and Notes

(1) Karger, J.; Ruthven, D. M. *Diffusion in Zeolites and other Microporous Solids*; Wiley-Interscience: New York 1992.
(2) Mitra, S.; Kamble, V. S.; Tripathi, A. K.; Gupta, N. M.; Mukhopadhyay. R. *Pramana* **2004**, *63*, 443.
(3) Sahasrabudhe, A.; Mitra, S.; Tripathi, A. K.; Mukhopadhyay R.; Gupta, N. M. *Phys. Chem. Chem. Phys.* **2003**, *5*, 3066.
(4) Sahasrabudhe, A.; Mitra, S.; Tripathi, A. K.; Mukhopadhyay, R.; Gupta, N. M. *J. Phys. Chem. B* **2002**, *106*, 10923.
(5) Mitra, S.; Tripathi, A. K.; Gupta N. M.; Mukhopadhyay, R. *Appl. Phys. A* **2002**, *74*, S1308.
(6) Sahasrabudhe, A.; Kamble, V. S.; Tripathi A. K.; Gupta, N. M. *J. Phys. Chem. B* **2001**, *105*, 4374.
(7) Tripathi, A. K.; Sahasrabudhe, A.; Mitra, S.; Mukhopadhyay, R.; Gupta, N. M.; Kartha, V. B. *Phys. Chem. Chem. Phys.* **2001**, *3*, 4449.
(8) Kamble, V. S.; Gupta, N. M. *Phys. Chem. Chem. Phys.* **2000**, *2*, 2661.
(9) Kamble, V. S.; Gupta, N. M. *J. Phys. Chem. B* **2000**, *104*, 4588.
(10) Shete, B. S.; Kamble, V. S.; Gupta, N. M.; Kartha, V. B. *Phys. Chem. Chem. Phys.* **1999**, *1*, 191.
(11) Shete, B. S.; Kamble, V. S.; Gupta, N. M.; Kartha, V. B. *J. Phys. Chem. B* **1998**, *102*, 5581.
(12) Kamble, V. S.; Gupta, N. M.; Kartha, V. B.; Iyer, R. M. *J. Chem. Soc., Faraday Trans.* **1993**, *89*, 1143.
(13) Mirth, G.; Kogelbauer, A.; Lercher, J. A. In *Proceedings of the 9th International Zeolite Conference*; von Ballmoos, R., Higgins, J. B., Treacy, M. M. J., Eds.; Butterworth-Heinemann: Boston, MA, 1993; p 251.
(14) Mukhopadhyay, R.; Mitra, S.; Paranjpe, S.; Dasannacharya, B. A. *Nucl. Instrum. Methods A* **2001**, *475*, 55.
(15) Jentys, A.; Pham, N. H.; Vinek, H. *J. Chem. Soc., Faraday Trans.* **1996**, *92*, 3287.
(16) Zhao, X. S.; Lu, G. Q.; Whittaker, A. K.; Millar, G. J.; Zhu, H. Y. *J. Phys. Chem. B* **1997**, *101*, 6525.
(17) Rep, M.; Palomares, A. E.; Eder-Mirth, G.; van Ommen, J. G.; Rosch, N.; Lercher, J. A. *J. Phys. Chem. B* **2000**, *104*, 8624.
(18) Corma, A. *Chem. Rev.* **1995**, *95*, 559.
(19) (a) Mirth, G.; Lercher, J. A. *J. Phys. Chem.* **1991**, *95*, 3736. (b) Mirth, G.; Lercher, J. A.; Anderson, M. W.; Klinowski, J. *J. Chem. Soc., Faraday Trans.* **1990**, *86*, 3039.
(20) Bée, M. *Quasielastic Neutron Scattering*; Adam-Hilger: Bristol, 1988.
(21) Press, W. *Single Particle Rotations in Molecular Crystals*; Springer: Berlin, 1981.
(22) Chudley, C. T.; Elliott, R. *J. Proc. Phys. Soc.* **1961**, *77*, 353.
(23) Hurle, R. L.; Easteal, A. J.; Woolf, L. A. *J. Chem. Soc., Faraday Trans. 1* **1985**, *81*, 769.
(24) Bermejo, F. J.; Batállan, F.; Enciso, E.; White, R.; Dianoux A. J.; Howells, W. S. *J. Phys. Condens. Matter* **1990**, *2*, 1301.
(25) Rathbun, R. E.; Babb, A. L. *J. Phys. Chem.* **1961**, *65*, 1072.
(26) Jobic, H.; Bée, M.; Kärger, J.; Vartapetian, R. S.; Balzer, C.; Julbe, A *J. Membrane Sci.* **1995**, *108*, 71.
(27) Flego, C.; Carati, A.; Perego, C. *Microporous Mesoporous Mater.* **2001**, *44*−*45*, 733.
(28) Kubelková, L.; Novaková, J.; Nedomová, K. *J. Catal.* **1990**, *124*, 441.
(29) Zecchina, A.; Bordiga, S.; Spoto, G.; Scarano, D.; Spano, G.; Geobaldo, F. *J. Chem. Soc., Faraday Trans.* **1996**, *92*, 4863.
(30) Pelmenschikov, A. G.; Morosi, G.; Gamba, A.; Zecchina, A.; Bordiga, S.; Paukshtis, E. A. *J. Phys. Chem.* **1993**, *97*, 11979.
(31) Pelmenschikov, A. G.; Morosi, G.; Gamba, A. *J. Phys. Chem.* **1992**, *96*, 2241.
(32) Hunger, B.; Matysik, S.; Heuchel, M.; Einicke, W.-D. *Langmuir* **1997**, *13*, 6249.
(33) Ritter, M. B.; Awschalom, D. D.; Shafer, M. W. *Phys. Rev. Lett.* **1988**, *61*, 966.
(34) Zerda, T. W.; Shao, Y. *Chem. Phys. Lett.* **1993**, *209*, 247.
(35) Mu, R.; Malhotra, V. M. *Phys. Rev. B* **1991**, *44*, 4296.
(36) Machin, W. D. *Langmuir* **1994**, *10*, 1235.
(37) Rathousky, J.; Zukal, A.; Franke, O.; Schulz-Ekloff, G. *J. Chem. Soc. Faraday Trans.* **1995**, *91*, 937.
(38) McLaughlin, E.; Ubbelohde, A. R. *Trans. Faraday Soc.* **1958**, *54*, 1804.